Synthesis and Characterization of Titania Nanostructures on Glass by Al Anodization and Sol−Gel Process

Song-Zhu Chu,* Kenji Wada, Satoru Inoue, and Sin-ichi Todoroki

Advanced Materials Laboratory, National Institute for Materials Science, Namiki-1, Tsukuba, Ibaraki, 305-0044, Japan

Received June 19, 2001. Revised Manuscript Received October 10, 2001

Titania nanostructures with larger surface areas are fabricated on a glass substrate by anodization of sputtered aluminum and the sol−gel process, and the structural characteristics of the nanostructures are investigated. Highly pure aluminum film (99.99%, ≈2 μm), which is deposited on a glass substrate with a conductive tin-doped indium oxide (ITO) layer, is first anodized potentiostatically in a phosphoric acid solution to obtain porous alumina structures. The anodic alumina is then used as a host or template to synthesize porous Al_2O_3/TiO_2 composite nanostructures through a sol−gel process. Finally, a TiO_2 nanotubules array with contours of porous anodic alumina is fabricated on glass by removing the alumina template selectively. The resultant TiO_2 is 4−20 nm polycrystalline of anatase structure with (101) preferential orientation. Titania nanostructures have large surface areas and exhibit a high transmittance in visible light and a strong absorbance within ultraviolet range in UV−vis spectra. Moreover, the fabrication of composite TiO_2−$x$$SiO_2$−$x$$TeO_2$ (x = 2.5%, 5%) nanostructures is also investigated. Addition of appropriate SiO_2 and TeO_2 to TiO_2 enhances not only the adhesion to the substrate but also the mechanical strength of the nanotubules, while showing little effect on the crystallinity and the UV−vis absorbance of TiO_2.

Introduction

Nanomaterials have attracted great interest in their potential applications in various fields such as electronics, magnetism, optics, and energy storage or exchange because they exhibit a broad range of enhanced mechanical, optical, magnetic, and electronic properties compared to coarser-grained materials with the same chemical composition.[1−2] So far, a variety of nanostructures (tubes, rods, fibers, or wires) of semiconductors,[3−8] carbons,[9−10] metals,[11−14] and other solid oxide materials[15−18] have been synthesized by utilizing a commercial porous alumina membrane as a template, which is obtained by anodizing an aluminum plate in acidic solutions under certain conditions.[19−21] Various techniques, such as chemical vapor deposition,[8,10,18] sol−gel deposition,[3,5−7,15−17] chemical polymerization,[4] and sintering[9,18] and electro-[11] and/or electroless deposition[12−14] have been adopted as major template synthetic strategies. Applications in broad fields such as photocatalysis, biosensors, molecular separators, and electronic devices are also being explored.[4,6,9,11]

Titanium dioxide has been well-known as a semiconductor with photocatalytic activities and applied in fields such as environmental purification, decomposition of carbonic acid gas, and utilization of solar energy.[22−32] The key factor in determining the photocatalytic activity

* To whom correspondence should be addressed. E-mail: CHU.Songzhu@nims.go.jp.

(1) Martin, C. R. *Science* **1994**, *266*, 1961.
(2) Huczko, A. *Appl. Phys. A* **2000**, *70*, 365.
(3) Lakshmi, B. B.; Dorhout, P. K.; Martin, C. R. *Chem. Mater.* **1997**, *9*, 857.
(4) Hulteen, J. C.; Martin, C. R. *J. Mater. Chem.* **1997**, *7* (7), 1075.
(5) Lakshmi, B. B.; Patrissi, C. J.; Martin, C. R. *Chem. Mater.* **1997**, *9*, 2544.
(6) Shelimov, K. B.; Moskovits, M. *Chem. Mater.* **2000**, *12*, 250.
(7) Zhang, M.; Bando, Y.; Wada, K. *J. Mater. Sci. Lett.* **2001**, *20*, 167.
(8) Cheng, G. S.; Chen, S. H.; Zhu, X. G.; Mao, Y. Q.; Zhang, L. D. *Mater. Sci. Eng.* **2000**, *A286*, 165.
(9) Kyotani, T.; Pradhan, B. K.; Tomita, A. *Bull. Chem. Soc. Jpn.* **1999**, *72*, 1957.
(10) Che, G.; Lakshmi, B. B.; C. J.; Fisher, E. R.; Martin, C. R. *Nature* **1998**, *393/28*, 346.
(11) Masuda, H.; Tanaka, H.; Baba, N. *Bull. Chem. Soc. Jpn.* **1993**, *66*, 305.
(12) Li, J.; Moskovits, M.; Haslett, M. L. *Chem. Mater.* **1998**, *10*, 1963.
(13) Shingubara, S.; Okino, O.; Sayama, Y.; Sakaue, H.; Takahagi, T. *Solid-State Electron.* **1999**, *43*, 1143.
(14) Cepak, V. M.; Hulteen, J. C.; Che, G.; Jirage, K. B.; Lakshmi, B. B.; Fisher, E. R.; Martin, C. R. *J. Mater. Res.* **1998**, *13*, 3070.
(15) Hirai, S.; Shimakage, K.; Aizawa, S.; Wada, K. *J. Am. Ceram. Soc.* **1998**, *81* (12), 3087.
(16) Shi, G.; Mo, C. M.; Cai, W. L.; Zhang, L. D. *Solid State Commun.* **2000**, *115*, 253.
(17) Zhang, M.; Bando, Y.; Wada, K.; Kurashima, K. *J. Mater. Sci. Lett.* **1999**, *18*, 1911.
(18) Pender, M. J.; Sneddon, L. G. *Chem. Mater.* **2000**, *12*, 280.
(19) Furneaux, R. C.; Rigby, W. R.; Davidson, A. P. *Nature* **1989**, *337*, 147.
(20) Masuda, H.; Fukuda, K. *Science* **1995**, *268*, 1466.
(21) Jessensky, O.; Müller, F.; Gösele, U. *J. Electrochem. Soc.* **1998**, *145*, 3735.
(22) Burnside, S. D.; Shklover, V.; Barbè, C.; Comete, P.; Arendse, F.; Brooks, K.; Grätzel, M. *Chem. Mater.* **1998**, *10*, 2419.
(23) Kasuga, T.; Hiramatsu, M.; Hirano, M.; Honson, A. *J. Mater. Res.* **1997**, *12*, 607.
(24) Kato, K.; Niihara, K. *Thin Solid Films* **1997**, *298*, 76.
(25) Kumar, P. M.; Badrinarayanan, S.; Sastry, M. *Thin Solid Films* **2000**, *358* (1−2), 122.

10.1021/cm0105918 CCC: $22.00
Published on Web 01/04/2002

of titanium dioxide lies in its specific surface area. To seek for large specific surface area, TiO_2 materials had been prepared as particle,[22,23] thin films[24−28] with rough surface or porous networks, nanotubules,[3−5,17,29,30] nanofibers,[7,31,32] etc. However, many concrete problems in applications for practical devices, such as the strength of tailored TiO_2 nanomaterials and the assembly for devices, have not been solved well yet.

Therefore, in this study, we attempt to create a novel technology to fabricate TiO_2 nanostructures with large surface area directly on a glass substrate by combining techniques of aluminum anodization and the sol−gel process. This approach is expected to have applications in manufacturing practical devices or functional glass for photocatalysis and/or solar energy utilization. In the present paper, the synthesis of TiO_2 nanostructures on a glass substrate by successive aluminum anodization and the sol−gel process is described, and the structural characteristics and the UV−visible absorbability of TiO_2 nanostructures are investigated. Moreover, from the viewpoint of application, to improve the mechanical strength of TiO_2 nanostructures and their adhesion to the substrate, the synthesis of composite TiO_2−SiO_2−TeO_2 nanostructures on glass and the effects of the addition of SiO_2 and TeO_2 to TiO_2 are also investigated.

Experimental Section

Specimens and Solutions. Highly pure aluminum (99.99%, ≈2 μm) was deposited on a glass substrate (soda lime glass, 20 × 100 × 1.1 mm) with an ITO film (100−130 nm, ≈20 Ω/□) and SiO_2 (≈15 nm) films. Aluminum deposition was performed by RF sputtering in a multicycled mode at a rate of 1.5 nm/s.

All the solutions were prepared with analytic-grade reagents and distilled water. The TiO_2 sol (≈5 wt %) used in the sol−gel process was prepared by titanium isopropoxide (TI), acetylacetone (ACAC), distilled water, and ethanol (EtOH) at a mole ratio of 1:1:3:20. The synthesis was carried out at room temperature in the open air. After being stirred at room temperature for 2 h, the TiO_2 sol was kept in a brown glass bottle at room temperature. The sol was very stable. The viscosity of the sol was at 2.36−2.40 centistokes (cSt −20 °C) without precipitation even for more than 2 months, though the color of the sol changes gradually from light yellow to dark yellow because of aging. In the experiments, the sols aged for 1 week to 1 month were used in the sol−gel process.

In another experiment, SiO_2−TeO_2 sol (≈5 wt %) was synthesized by tetraethyl orthosilicate (TEOS), telluric acid, EtOH, H_2O, and HCl at a mole ratio of 1:1:20:4:0.03. In fabrication of composite TiO_2−SiO_2−TeO_2 nanostructures, 5−10% (wt) of SiO_2−TeO_2 sol was added to the TiO_2 sol.

Synthetic Methods of TiO_2 Nanostructures. After ultrasonic cleaning in acetone for 10 min, the specimens were anodized potentiostaticly in a 10% (vol) phosphoric acid solution at 60−150 V and 4−10 °C to obtain porous alumina structures with unit cell sizes in 110−450 nm. The anodized specimens were then immersed in a 5% (vol) phosphoric acid solution at 30 °C for 15−45 min to enlarge the pore size and remove the barrier layer of anodic alumina films.

In sol−gel coating, the anodic alumina structures were first immersed in ethanol for 10 min and then dipped into the TiO_2 sol at room temperature for 20 min. The withdrawal speed in dip coating was not controlled. For UV−vis spectra measurement, the TiO_2 gel on the back of the specimens (glass side) was washed away with ethanol. After drying in the air at room temperature for more than 2 h, the specimens were heated in the air in a muffle furnace (SIBATA: CM-200) at 100 °C for 1 h and 400 °C for 2 h, at a rate of 2 °C/min, to obtain porous Al_2O_3/TiO_2 nanostructures. Titania nanotubules array on glass was finally obtained after removing a surface TiO_2 layer by mechanical abrading and after removing anodic alumina by chemical etching in a solution containing 5% H_3PO_4 and 2% CrO_3 at 75 °C for 5−8 min.

Characterizations. The morphology of the surface and the fracture cross section of the specimens were observed by a field emission scanning electron microscope (FESEM: S-5000, Hitachi) with an energy-dispersive X-ray analyzer (EDX) after osmium evaporation.

Transmission electron microscopy (TEM: JEOL-100V) was used to observe the crystal structure of the TiO_2 layer and to determine the size of the crystals. The specimens after sol−gel coating were embedded into epoxy resin and cut by an ultramicrotome (LKB-2088/V) with a diamond knife into ≈60 nm thick slices. The sliced specimens were set on carbon-coated copper grids and observed at 100 kV in the bright field mode along with the corresponding diffraction patterns. The crystallization and phase structure of TiO_2 nanostructures were analyzed by an X-ray diffractometer (XRD: RINT-2200V/PC, Cu Kα, 40 V/40 mA). The UV−visible spectra of the specimens were measured in the transmission mode by a spectrometer (U-3500, Hitachi) at a resolution of 2 nm.

Results and Discussion

Formation of a Porous Anodic Alumina Structure on Glass. A porous alumina structure with uniform and parallel channels on a glass substrate is essential for fabricating nanostructures within the pores because the contours of nanostructures follow the pore walls of an anodic alumina template. Figure 1 shows the FESEM images of a fracture section of porous anodic alumina films obtained at different anodic potentials and temperatures. At lower potentials such as 60 V, the porous anodic alumina film is composed of discontinuous pores with many branches, especially at the interface zones caused by a multicycled sputtered aluminum layer. With increasing anodizing potential, the pores of the films become straight with fewer branches and arrange in a direction perpendicular to the substrate. At potentials higher than 130 V, porous alumina structures with uniform and almost parallel pores are obtained.

Figure 2 shows the changes of (a) thickness (δ_a), and (b) pore diameter and pore interspace of anodic alumina films with anodizing potential (E_a) for anodization of a sputtered aluminum layer 2 μm thick, which are measured and calculated based on the photos in Figure 1. In Figure 1a, the thickness of anodic alumina films increases as the anodizing potential increases, irrespective of the anodizing temperature. At potentials between 60 and 110 V, the film thickness increases linearly with the anodizing potentials, while reaching 130 V, the increment of film thickness becomes larger suddenly. This behavior corresponds exactly to the transition of the pore arrangement of the anodic alumina films, that is, in a direction perpendicular to the substrate from 130 V (see Figure 1). The thickness ratio of the anodic oxide film and the sputtered aluminum layer, $\delta_{Al_2O_3}/\delta_{Al}$,

(26) Kato, K.; Torii, Y.; Taoda, H.; Kato, K.; Butsugan, Y.; Niihara, K. *J. Mater. Sci. Lett.* **1996**, *15*, 913.
(27) Enright, B.; Fitzmaurice, D. *J. Phys. Chem.* **1996**, *100*, 1027.
(28) Caruso, R. A.; Antonietti, M.; Giersig, M.; Hentze, H. P.; Jia, J. *Chem. Mater.* **2001**, *13*, 1114.
(29) Kasuga, T.; Hiramatsu, M.; Hoson, A.; Sekino, T.; Niihara, K. *Langmuir* **1998**, *14*, 3160.
(30) Imai, H.; Takei, Y.; Shimizu, K.; Matsuda, M.; Hirashima, H. *J. Mater. Chem.* **1999**, *9* (12), 2971.
(31) Hoyer, P.; Masuda, H. *J. Mater. Sci. Lett.* **1996**, *15*, 1228.
(32) Imai, H.; Matsuda, M.; Shimizu, K.; Hirashima, H.; Negishi, N. *J. Mater. Chem.* **2000**, *10*, 2005.

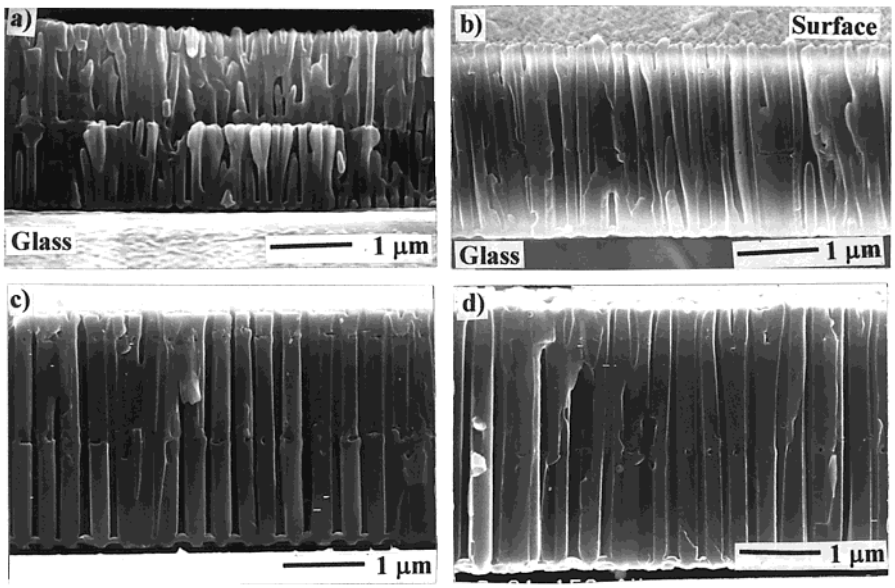

Figure 1. FESEM images of a fracture section of anodic alumina films anodized at the following conditions: (a) 60 V, 10 °C, 15 min; (b) 110 V, 7 °C, 100 min; (c) 130 V, 7 °C, 60 min; and (d) 150 V, 4 °C, 35 min.

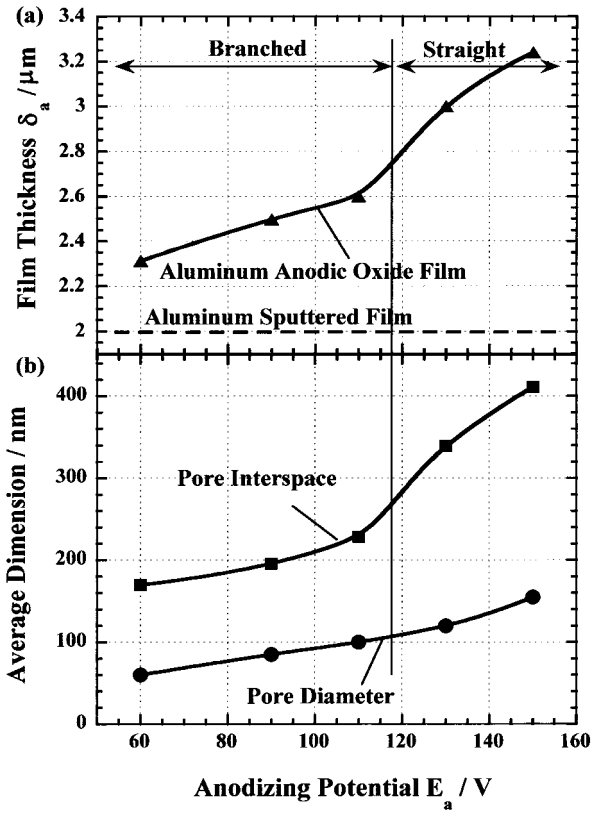

Figure 2. Relationship of (a) the thickness (δ_a), and (b) pore size (ϕ) and cell size of anodic alumina films, with the anodizing potential (E_a) for the anodization of aluminum sputtered on a glass substrate with an ITO film.

changes from 1.15 at 60 V to 1.65 at 150 V, meaning that higher potentials lead to form thicker anodic oxide films. The effect of anodizing potentials on the thickness of anodic alumina films could be ascribed to the highly ordered pore arrangement of anodic alumina films at higher potentials and/or the electrochemical dissolution of aluminum during anodization, even though more investigations are needed to elaborate the mechanism. This result is observed and reported in the present study for the first time, even though the volume expansion of anodic oxide films has been known for many years.

Similar to anodization of bulk aluminum plates or foils,[19−21] the anodizing potential also affects the pore diameter and the pore interspace of anodic alumina (Figure 2b). Higher potentials lead to porous alumina films with a larger pore size and pore interspace, and the latter is relevant to the pore density of anodic alumina. On the basis of our calculations from FESEM images of surface morphology (not shown), the pore density of the anodic alumina structures obtained in this study is $\approx 1.0-7.4 \times 10^{13}$ pore/m^2; that is, the resultant porous anodic alumina structures have large surface areas.

Synthesis of TiO_2 Nanostructures on Glass. Porous anodic alumina films after pore widening (Figure 3a) are used as a template to synthesize TiO_2 nanostructures through sol−gel deposition. Figure 3 shows the FESEM images of (b) fracture sections and (c) a bottom view of a Al_2O_3/TiO_2 composite layer synthesized on the anodic alumina obtained at 150 V. It can be seen from Figure 3b that the TiO_2 layer in the pores is basically uniform and the channels remain hollow throughout the films, even though some gel particles exist in some pores. Comparing Figure 3c with Figure 3a exhibits clearly the hollow TiO_2 gel structures within the pores of anodic alumina down to the substrate. The TiO_2 layer in the pores is dense without cracks and adheres tightly to the pore walls (see the arrows). This indicates that the TiO_2 sol flows into the pores along the pore walls of anodic alumina in the dip coating because of the surface tension and the capillary effect. It should be mentioned that the affinitive treatment in ethanol for anodic alumina prior to dip coating is an indispensable step for achieving hollow TiO_2 gel structures; otherwise, a solid structure with voids is acquired because of the shrink stress in the drying and heating of the TiO_2 gel. It was also found that hollow TiO_2 gel structures could be acquired for all the porous alumina structures in Figure 1, while the anodic alumina with a small pore size (e.g., 60 V) led to a TiO_2 gel layer with

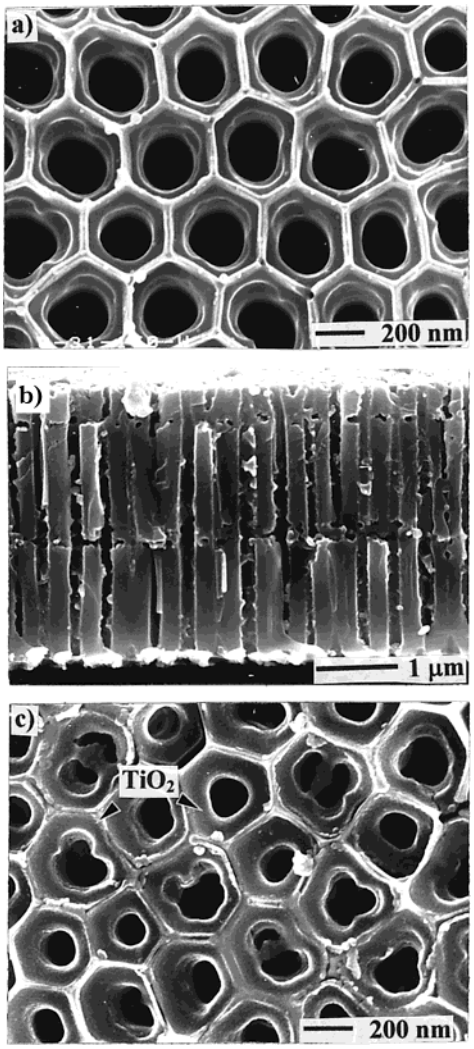

Figure 3. FESEM images of (a) a bottom view of anodic alumina film after pore widening and before sol−gel coating, (b) a fracture section, and (c) a bottom view of a Al_2O_3/TiO_2 composite layer after dip coating and heating at 400 °C for 2 h. Before imaging, the specimen (b) was mechanically abraded with diamond paste to remove the TiO_2 layer on the composite layer. The bottom views of the specimens (a) and (c) were obtained by stripping the membranes mechanically from the substrate at the membrane/ITO interfaces and setting reversibly on the holder. (Anodizing: 150 V, 4 °C, 35 min. Pore widening: 45 min.)

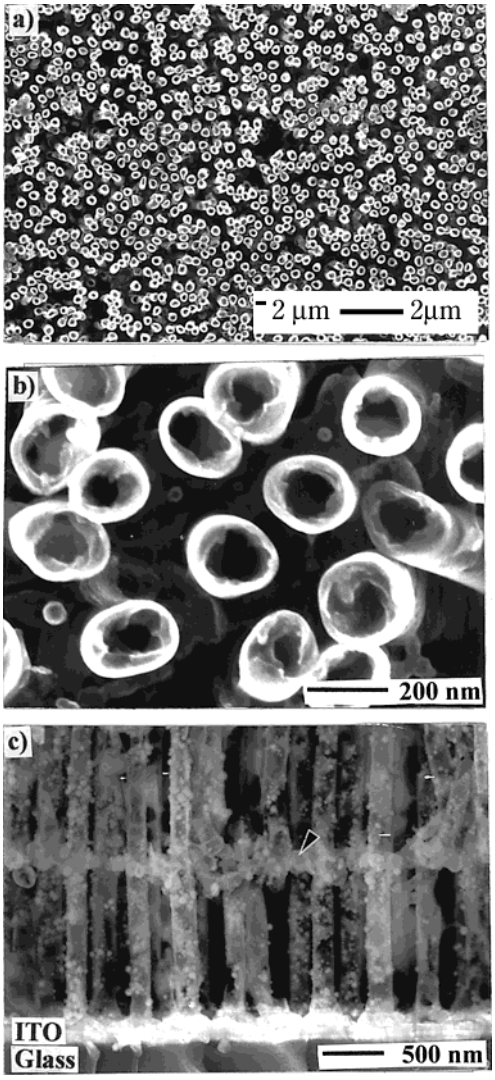

Figure 4. FESEM images of (a) and (b) TiO_2 (top view) and (c) TiO_2−2.5%SiO_2−2.5%TeO_2 (side view) nanotubules arrays standing on a glass substrate after removal of anodic alumina by selective chemical etching in a solution of 5% H_3PO_4 and 2% CrO_3 at 75 °C for 5−8 min. The conditions of anodization and pore widening are the same as those in Figure 3.

thinner walls, possibly caused by the small volume of TiO_2 sol entered in the pores.

After the anodic alumina is removed by selective chemical etching, a nanostructure of a TiO_2 nanotubules array on a glass substrate is achieved. Figure 4 gives an example of a TiO_2 nanotubules array on the glass substrate synthesized upon the anodic alumina structures obtained at 150 V. The TiO_2 nanotubules stand straight on the glass substrate with an ITO film due to the good adherence between the nanotubules and the underlying ITO film. Good adherence could be accounted for by the strong joining force of covalent oxo bridges (>X−O−Ti<; X = In, Sn). The nanotubules are separate from each other with certain spaces, where the anodic alumina template had been. This makes it possible to expose the whole outer surface of the nanotubules to the atmosphere. Titania nanotubules are ≈3.0 μm long (because of the mechanical abrasion) and 200−233 nm in outer diameter with a wall thickness of 30−53 nm. The outer diameter and surface of TiO_2 nanotubules follow faithfully the inner ones of the pores of anodic alumina before sol−gel coating (Figure 3a), while the inner surface is not so smooth because of the shrinking of the gel, thus leading to the TiO_2 tubules with uneven walls.

It was also found that, however, the Al_2O_3/TiO_2 composite layers were partly detached at the interface of the Al_2O_3/TiO_2 layer and the ITO/glass substrate when the specimens were cut with a glass knife (Figures 3b and 3c) and that part of the TiO_2 nanotubules broke off at the interface zone of anodic alumina films after etching. This is an essential problem in manufacturing practical devices of TiO_2 nanostructures on glass substrates. Therefore, to improve the strength of TiO_2 nanostructures and the adhesion to the substrate, we attempted to synthesize composite TiO_2−SiO_2−TeO_2 nanostructures on the glass substrate by the same approach. Here, SiO_2 is adopted because of its high mechanical strength and excellent corrosion resistance and TeO_2 is used because of its low glass transition

temperature (≈380 °C).[33] Figure 4c gives an example of a composite $TiO_2-2.5\%SiO_2-2.5\%TeO_2$ nanotubules array on a glass substrate. The nanotubules stand rigidly on the substrate, with a smooth outer surface and a rough inner surface like the TiO_2 ones. The interesting thing is that the composite $TiO_2-SiO_2-TeO_2$ even fills into the interface zones of anodic alumina (see the arrow) and makes a strong connection among the nanotubules, thus forming an integrated "network" structure and leading to a sturdy unity of the nanotubules array on glass. Moreover, it was also found that the adhesion to the substrate, the mechanical strength, and the chemical stability of $TiO_2-SiO_2-TeO_2$ nanotubules increase with the content of SiO_2 and TeO_2 in TiO_2. The effects of adding SiO_2 and TeO_2 could be ascribed to the strong covalent bonds of oxo bridges (>X−O−Y<; X = In, Sn; Y = Ti, Si, Te)[34,35] and/or, more possibly, the intergranular glass phase films of SiO_2 or TeO_2 (refer to XRD results in Figure 5 later) at the grain boundaries between crystalline TiO_2 and In_2O_3, according to Clarke et al.[36,37] The intergranular glassy films of SiO_2 and TeO_2 in TiO_2 could also contribute to the good mechanical strength and chemical stability of the composite nanotubules. However, a comprehensive discussion on the functions of SiO_2 and TeO_2 in TiO_2 will be done after some additional experiments in a future work and so are not elaborated on in the present paper.

Structure Analysis of Titania Nanostructures. Figure 5 shows the X-ray diffraction patterns of $Al_2O_3/TiO_2-xSiO_2-xTeO_2$ (x = 0, 2.5%, 5%) composite layers obtained by sol−gel coating (4 times) and heating at 400 °C for 2 h. The X-ray diffraction pattern of the TiO_2 layer (a) shows several peaks at 25.3°, 37.8°, 48.0°, 54.0°, 55.0°, and 62.7°, inferring the crystallization and polycrystalline structure of the TiO_2 layer. According to their positions, the peaks are identified as the anatase phase of titanium oxide. The TiO_2 crystals exhibit a preferential orientation in a (101) facet, which are thought to have good performance in photocatalysis. The X-ray patterns of $TiO_2-2.5\%SiO_2-2.5\%TeO_2$ composite layers (b) show several characteristic peaks of anatase TiO_2 at 25.3°, 37.8°, 48.0°, and 54.0°, even though the intensity of the peaks is weaker than those of the pure TiO_2 layer; while for $Al_2O_3/TiO_2-5\%SiO_2-5\%TeO_2$ composite layers (c), only a weak peak at 25.3° (anatase−(101) facet) appears. This fact suggests that adding excessive SiO_2-TeO_2 to TiO_2 retards the crystallization of TiO_2 to some extent, even though it shows no effect on the phase structure of anatase TiO_2. In addition, no peak corresponding to SiO_2 or TeO_2 is found in the patterns because SiO_2 and TeO_2 are in an amorphous or glass state at 400 °C.

As reference, XRD patterns for anodic alumina film (d) and sputtered aluminum film (e) are also given in Figure 5. The sputtered aluminum films here are the polycrystalline with strong orientation in a (111) facet. This is different from commercial bulk aluminum plates,

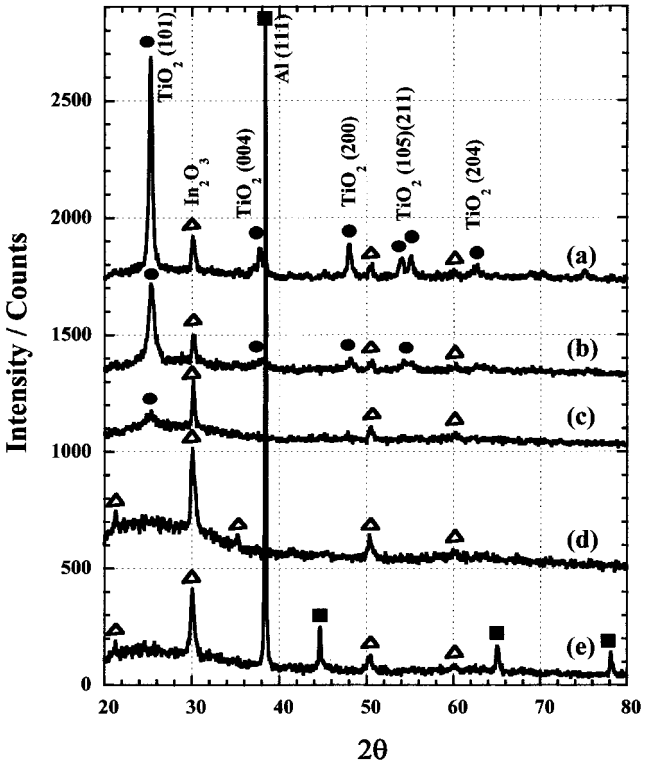

Figure 5. X-ray diffraction patterns of composite layers (a) Al_2O_3/TiO_2, (b) $Al_2O_3/TiO_2-2.5\%SiO_2-2.5\%TeO_2$, and (c) $Al_2O_3/TiO_2-5\%SiO_2-5\%TeO_2$ obtained by sol−gel coating (4 times) and heating at 400 °C for 2 h, (d) anodic alumina film anodized at 150 V, and (e) Al sputtered film on a glass substrate with an ITO film.

which are usually with preferential orientation in a (200) facet. After anodization (d), the peak corresponding to Al (111) disappeared completely because all of the aluminum metal transferred into the oxide. Also, no peak corresponding to crystalline Al_2O_3 is found in the pattern, indicating that the anodic alumina is still in an amorphous state, even at such a high anodizing potential of 150 V. In all the patterns, peaks appeared at 30.1° and 50.3° are ascribed to In_2O_3 from ITO films on glass substrates because of the thin thickness of deposited layers.

Figures 6a and 6b show the transmission electron microscopic (TEM) images of the (a) top and (b) bottom regions of the Al_2O_3/TiO_2 composite layer heated at 400 °C for 2 h. The granular TiO_2 is clearly seen, inferring a polycrystalline structure. The TiO_2 layer in the pores of anodic alumina is continuous and dense, even though parts of the layer have peeled off from the alumina walls in the preparation for TEM observation. The distributions of TiO_2 grain size corresponding to the different positions of the composite layer are plotted in Figure 6c. The dimensions of the grains are different with the positions of the composite layer: approximately 5−20 nm at the top and 4−10 nm at the bottom, respectively. In other words, the TiO_2 gains tend to be finer and the grain distribution becomes narrower, from top to bottom of the porous alumina film, that is, along the flowing route of TiO_2 solution in the dip coating. The finer grains of the TiO_2 within the nanopores compared to those of the top layer could be ascribed to either the effect of the pore walls on the nucleation and growth of TiO_2 crystals or the thinner solution of TiO_2 in the pores, where wetted by ethanol prior to the dip coating.

(33) Pye, L. D.; La Course, W. C.; Stevens, H. J. *The Physics of Non-Crystalline Solids*; Taylor & Francis: London/Washington, DC, 1992; p 281.
(34) West, A. R. *Basic Solid State Chemistry (Second Edition)*; John Wiley & Sons: Chichester, 1999.
(35) Samsonov, G. V. *The Oxide Handbook*; IFI/Plenum: New York, 1973.
(36) Clarke, D. R. *J. Am. Ceram. Soc.* **1987**, *70*, 15.
(37) Tanaka, I. *J. Ceram. Soc. Jpn.* **2001**, *109*, 127.

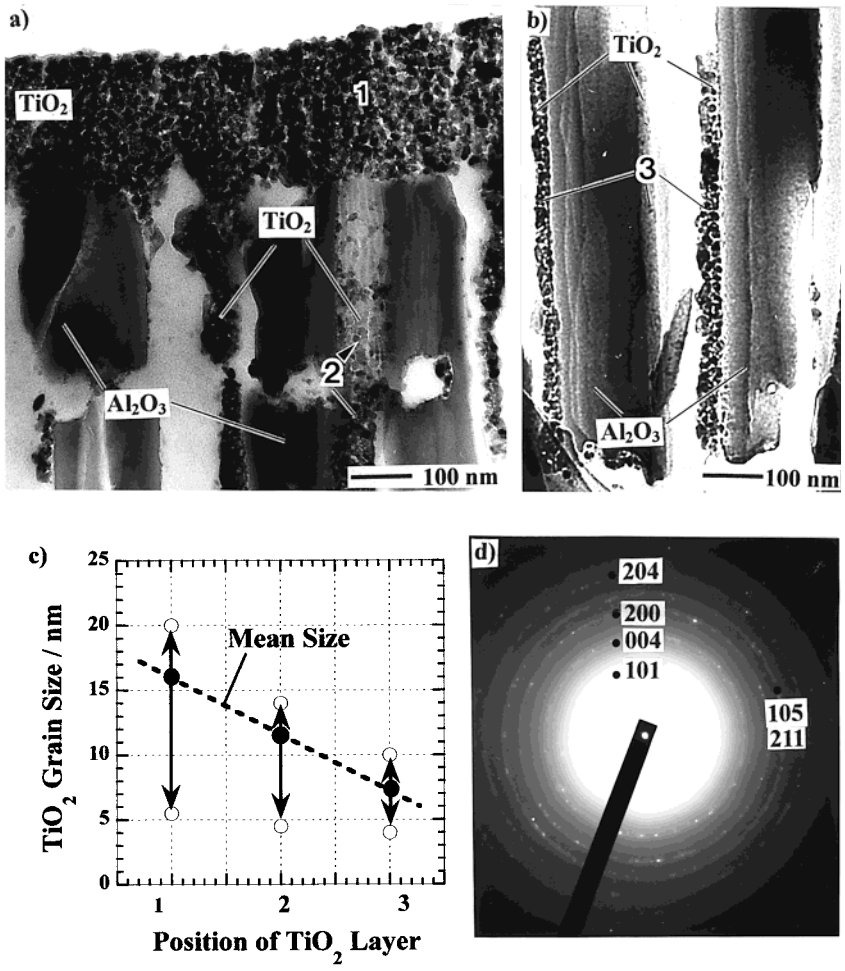

Figure 6. TEM images for the (a) top and (b) bottom of the Al_2O_3/TiO_2 composite layer after being heated at 400 °C for 2 h, (c) distribution of TiO_2 grain size, and (d) electron diffraction pattern of the upper TiO_2 layer. The conditions of anodization and pore widening are the same as those in Figure 3.

Figure 6d gives a typical electron diffraction pattern corresponding to the upper TiO_2 layer in Figure 6a. It shows several reflections that correspond closely to the (101), (004), (200), (105), (211), and (204) reflections of tetragonal anatase titanium oxide with the lattice constants $a = 3.78$ Å and $c = 9.58$ Å. All the reflections are continuous rings, indicating that the TiO_2 layer is highly crystalline and has a polycrystalline structure. This result is consistent with the results of XRD analysis. Moreover, the $TiO_2-2.5\%SiO_2-2.5\%TeO_2$ composite layer was also investigated by TEM observation. The grain size and the diffraction pattern are similar to those of the TiO_2 layer, indicating that the addition of a small amount of SiO_2-TeO_2 to TiO_2 has almost no effect on the crystal structure of TiO_2. This, again, is consistent with the results of XRD analysis (Figure 5).

UV−Visible Absorption Spectra of Titania Nanostructures. Figure 7 shows the UV−visible transmittance spectra for specimens after anodization, sol−gel coating, and chemical etching. The anodic alumina films (solid line 1) are almost optically transparent, so the transparency of the composite layers is predominantly decided by the TiO_2 layers within the pores. The transmittances of the Al_2O_3/TiO_2 composite layer (dotted line 2) and the TiO_2 nanotubules array (solid line 3) are smaller than that of the anodic alumina film throughout the UV−visible range because of the absorbance of the TiO_2 layer or nanotubules. Nevertheless, the TiO_2 nanostructures still exhibit a relatively high transmittance (50−80% T) in the visible light range. Furthermore, all the TiO_2 nanostructures, porous layer or nanotubules array, show a strong absorbance (<30% T)

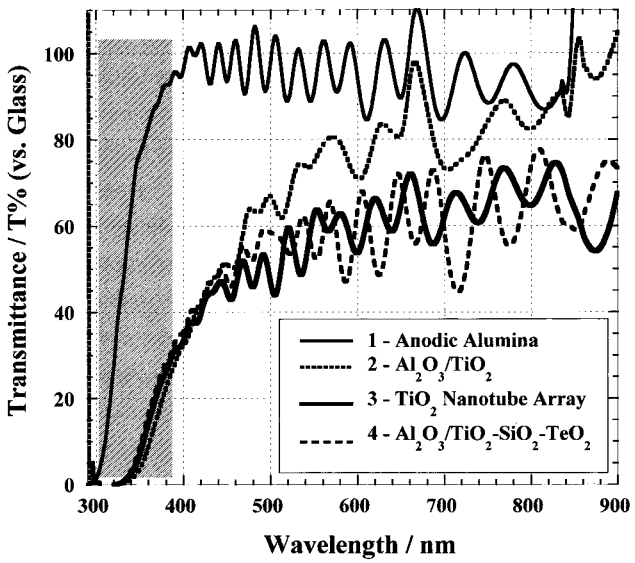

Figure 7. UV−visible transmittance spectra of specimens after anodization, sol−gel coating, and chemical etching. The conditions of anodization, pore widening, sol−gel coating, and alumina removal are the same as those in Figures 3 and 4.

at wavelengths below 400 nm (see batched area), inferring absorption of TiO_2 in the ultraviolet light range. It should be mentioned that even though the Al_2O_3/TiO_2 composite layer exhibits nearly the same absorbability in the UV light range as the TiO_2 nanotubules array, the latter would be related to higher photocatalytic performance because of the larger surface area. Moreover, the absorptive spectrum of the $TiO_2-2.5\%SiO_2-2.5\%TeO_2$ composite layer is also given in Figure 7 (dotted line 4). Little effect for the addition of SiO_2-TeO_2 on the UV−visible absorbance of TiO_2 nanostructures is found. In addition, a strong interference phenomenon is observed in all spectra. This could be ascribed to the porous structures of the layers and/or the thickness and the refractive index of the ITO film (100−130 nm; 2.0) and the SiO_2 film (≈15 nm; 1.4) on the glass substrate. The magnitude of the interference in the spectra becomes weaker after sol−gel coating, but becomes stronger again when anodic alumina is removed by chemical etching, possibly because of the block of TiO_2 layer to the interference light.

Surface Areas of Titania Nanostructures. Titania nanostructures on glass fabricated in the present study would have very large surface areas, which is incomparable for those conventional flat TiO_2 films. For instance, for porous Al_2O_3/TiO_2 composite structures, all the TiO_2 layers in the pores with an open entrance could be used as reacting sites, and for TiO_2 nanotubules array, both the inner side and the outer side of tubules could be utilized. Here, the surface areas of porous Al_2O_3/TiO_2 composite structures and TiO_2 nanotubules arrays can be calculated from the following equations,

$$S_1 = \pi\phi_{\text{inner}} h_1 D_{\text{pore}} + 1 \quad (\text{m}^2/\text{m}^2\ \square) \tag{1}$$

$$S_2 = \pi(\phi_{\text{inner}} + \phi_{\text{outer}}) h_2 D_{\text{pore}} + \pi(\phi_{\text{inner}}/2)^2 D_{\text{pore}} \quad (\text{m}^2/\text{m}^2\ \square) \tag{2}$$

where S_1 and S_2 represent the surface area of porous Al_2O_3/TiO_2 composite layers and TiO_2 nanotubules arrays compared to the unit area of the substrate, respectively. Value 1 in eq 1 is defined as the surface area of a flat film on the substrate. ϕ_{inner} and ϕ_{outer} are the inner pore diameter of porous layers or the inner and outer diameters of nanotubules, and h_1 and h_2 are the thickness of the porous composite layer and the height of nanotubules, respectively. D_{pore} is the pore density of the porous layer or the number of nanotubules per unit area. Therefore, from eqs 1 and 2, for the porous Al_2O_3/TiO_2 composite layer as in Figure 3b, the surface area is calculated as 18.2−22.2 m^2 compared to 1 m^2 of the glass substrate (ϕ_{inner} = 124−153 nm, h_1 = 3.4 μm, $D_{\text{pore}} = 1.3 \times 10^{13}$); while for the TiO_2 nanotubules array as in Figure 4a, the surface area is 40.2−47.1 m^2 compared to 1 m^2 of the glass substrate (ϕ_{inner} = 127−150 nm, ϕ_{outer} = 200−233 nm, h_2 = 3.0 μm, $D_{\text{pore}} = 1.3 \times 10^{13}$). Moreover, the surface area of TiO_2 nanostructures could also be adjusted by varying the parameters anodizing potential (D_{pore}), pore-widening period (ϕ), aluminum sputtering cycle (h), and so on.

Conclusions

Titania nanotubules arrays standing on glass substrates are successfully synthesized by anodization of sputtered aluminum and the sol−gel process. The TiO_2 nanotubules arrays have very large surface areas in several tens of square meters on a unit area glass substrate, which are dependent on the pore density of the anodic alumina templates formed. To achieve a porous alumina structure with parallel pores perpendicular to the substrate, the anodization of sputtered aluminum must be performed at potentials higher than 130 V, below which porous alumina with branch pores are formed. Titania heated at 400 °C is 4−20 nm polycrystalline of anatase structure with a preferential (101) facet. The TiO_2 nanostructures, both TiO_2 nanotubules arrays and porous Al_2O_3/TiO_2 composite layers, exhibit a high transmittance (50−80% T) in the visible range and a strong absorbance (below 30% T) in the ultraviolet light range.

From a practical viewpoint, composite $TiO_2-xSiO_2-xTeO_2$ (x = 2.5%, 5%) nanotubules arrays on glass are also synthesized by this approach. Adding an appropriate amount of SiO_2 (2.5%) and TeO_2 (2.5%) to TiO_2 not only improves the adhesion to the glass substrate but also enhances the mechanical strength and chemical stability of the titania nanostructures, without affecting the crystallinity and UV−vis absorption of TiO_2. Particularly, the composite $TiO_2-SiO_2-TeO_2$ can fill the interface zones of anodic alumina and make the separate nanotubules join into an integrated and sturdy "network" structure on glass. This makes it possible to fabricate longer TiO_2-based nanotubules on glass substrates with satisfying strength and larger surface areas.

Acknowledgment. This work is part of the Japan Millennium Project of "Search and Creation of a Catalyst for Removing Harmful Chemical Substances". The authors wish to thank the Asahi Glass Co., Ltd., for providing glass substrates with ITO films and Kyodo International Company for producing sputtered aluminum. The authors also wish to thank Mr. Y. Kitami for assisting in TEM observations.

CM0105918